Journal of the Optical Society of America B
OPTICAL PHYSICS

Maximizing the FWM conversion efficiency in a PCF with a randomly varying pitch

Wei Zhang,[1] Rafael R. Gattass,[2] L. Brandon Shaw,[2] Curtis R. Menyuk,[3] and Jonathan Hu[1,*]

[1]Baylor University, One Bear Pl. #97356, Waco, Texas 76798, USA
[2]Naval Research Laboratory, Code 5620, Washington DC, 20375, USA
[3]University of Maryland Baltimore County, 5200 Westland Blvd., Baltimore, Maryland 21227, USA
*Jonathan_hu@baylor.edu

Received 29 July 2024; revised 12 September 2024; accepted 15 September 2024; posted 16 September 2024; published 1 October 2024

We theoretically investigate the generation of visible light using four-wave mixing (FWM) in photonic crystal fibers (PCFs), whose input is produced by a high-power continuous wave (CW) or quasi-CW fiber laser. We analyze the impact on the conversion efficiency of the randomly varying pitch along the fiber, which in turn leads to variations of the FWM wavelength. We show that the conversion efficiency is maximized when the mean pitch and hole diameters are chosen so that the derivative of the FWM wavelength with respect to the pitch is zero. We then use this criterion to determine the maximum conversion efficiency over a wavelength range of 650–850 nm with a pump at 1064 nm.

https://doi.org/10.1364/JOSAB.537104

1. INTRODUCTION

The development of fiber lasers has led to the commercialization of many lasers for military, medical, and industry applications [1–3]. However, the development of new laser sources at wavelengths that are not commercially available can be difficult and expensive. Hence, there is considerable interest in developing sources that can be tuned to cover a broad wavelength range using nonlinear wavelength conversion of the pump power from well-developed lasers. The ideal system should be compact and simple in order to provide a low-cost solution.

Parametric conversion using four-wave mixing (FWM) in optical fibers provides a mechanism for tunable wavelength conversion [4,5]. It is a simple system that combines a section of fiber and a high-power pump laser. A fiber laser, such as a Yb^{3+}-doped fiber laser, is an appropriate pump source for an all-fiber integrated, tunable laser source. An all-fiber system can avoid the issues with free space coupling while achieving high average power and tunability at visible wavelengths. For example, Wadsworth *et al*. [6] demonstrated more than 30% conversion of sub-nanosecond pulses from a Nd:YAG laser at 1064 nm to a signal at 732 nm in a single pass of a 3-m-long photonic crystal fiber (PCF). Lavoute *et al*. [7] demonstrated a conversion efficiency of 30% in a single pass system using fiber lengths less than 1 m. The combination of a Yb^{3+}-doped fiber laser system and a PCF can generate wide coverage of the red and near-IR light from 650 to 820 nm by suitably choosing the pitch and hole diameter of the PCF [7]. Other experiments have demonstrated tunable optical sources with a wavelength range that is greater than 400 nm by tuning the pump wavelength near the fiber zero-dispersion wavelength [8,9].

The FWM efficiency has a strong impact on fiber laser applications, and it plays an essential role in PCF-based fiber lasers [10]. In order to optimize the efficiency of the wavelength conversion when using a pump laser at 1064 nm, it is necessary to optimize the PCF geometry. PCFs with different pitches and hole diameters enable a wide variation of the dispersion dependence on wavelength. On the other hand, a small amount of variation in the air-glass interface also leads to large dispersion fluctuations along the fiber, compared to conventional step-index fibers [11]. Previous research has shown that the variation of the pitch along the length of PCFs can be as large as 1%–5% [12,13]. The effect of dispersion fluctuations on optical parametric amplification has been widely studied theoretically and experimentally [14–17]. The effect of randomly varying dispersion fluctuations has also been studied using numerical simulations to obtain values for the mean and variance of the parametric gain [11,17–19]. The dispersion fluctuations induced by the variation of the fiber pitch and hole diameter are hard to control when drawing the fiber, although the ratio of pitch to hole diameter is nearly constant [13,20,21]. Even though the stack-and-draw technique, which is commonly used to manufacture PCFs, is well developed, small variations in the fabrication process lead to variations in the pitch and hence the dispersion. The final FWM efficiency depends strongly on the variation of the pitch along the fiber—a variation that is

embedded during the fiber drawing [22]. The dispersion characteristics are particularly sensitive to the inevitable fabrication inaccuracies in fibers that have a small core diameter, as is commonly the case for fibers that are used for nonlinear wavelength conversion [22].

In this paper, we discuss an approach to minimize the impact of variations in the fiber geometry and hence maximize the wavelength conversion efficiency by appropriately choosing the mean values of the PCF fiber geometric parameters—the pitch Λ and the ratio of the hole diameter to the pitch d/Λ. We study the FWM conversion efficiency in the presence of dispersion fluctuations, assuming a random variation of Λ and a fixed ratio d/Λ. In this study, we consider a degenerate FWM process, where two photons from the pump wave generate one photon in both the signal and idler waves. Energy conservation in this process is described by the equation, $2\omega_p = \omega_s + \omega_i$, where ω_p is the angular frequency of the pump wave, $\omega_s = 2\pi c/\lambda_{\mathrm{FWM}}$ is the angular frequency of the signal wave, ω_i is the angular frequency of the idler wave, and c is the speed of light in vacuum [4,23]. We find that the conversion efficiency is maximized by choosing Λ and d/Λ so that the derivative of the four-wave mixing signal wavelength λ_{FWM} with respect to Λ equals zero, i.e., $d\lambda_{\mathrm{FWM}}/d\Lambda = 0$. In this paper, we write λ_{FWM} to denote the signal anti-Stokes wavelength at which we aim to generate high power. The choice of an optimal pitch Λ lowers the sensitivity of the FWM process to fiber variations and thus enhances its gain. We determine the geometric parameters that should be used to maximize the efficiency over a wide range of output visible wavelengths from 650–850 nm with a pump wavelength of 1064 nm.

2. FIBER DESIGN

In this section, we use the phase matching condition [7,24] to estimate the FWM signal wavelength with a power of 1 kW. We limited the PCF air hole cladding to five rings. We calculated the fiber modes and their propagation constants using COMSOL Multiphysics, a commercial full-vector mode solver that uses the finite-element method. Anisotropic, perfectly matched layers (PMLs) are positioned outside the cladding in order to reduce the size of the simulation window [25]. We show that contour plots of λ_{FWM} as Λ and d/Λ vary in Fig. 1. Pump wavelengths of 1064 nm and 1030 nm are used in Figs. 1(a) and 1(b), respectively. Both pump sources are widely used in experimental applications [10,26–29]. A similar figure was presented in Ref. [7] using a pump wavelength of 1064 nm. We use the phase matching condition [7,24] to find the fiber configuration when λ_{FWM} equals 750 nm, which is plotted as the red dashed curve. The black cross in Fig. 1(b) denotes the parameter for a measured NKT LMA-5 fiber [30]. This indicates that the NKT LMA-5 fiber can be used to perform wavelength conversion to generate the λ_{FWM} of 750 nm. Figure 1 serves as a visual guide to understand how changes in fiber design parameters can influence the phase matching condition for four-wave mixing, a nonlinear optical process crucial in applications like wavelength conversion and optical parametric amplification. Points "A" and "C" mark the condition where the derivative $d\lambda_{\mathrm{FWM}}/d\Lambda$ equals zero and $\lambda_{\mathrm{FWM}} = 750$ nm. If we slightly vary the pitch Λ, the derivative $d\lambda_{\mathrm{FWM}}/d\Lambda$ is no longer zero according to Fig. 1.

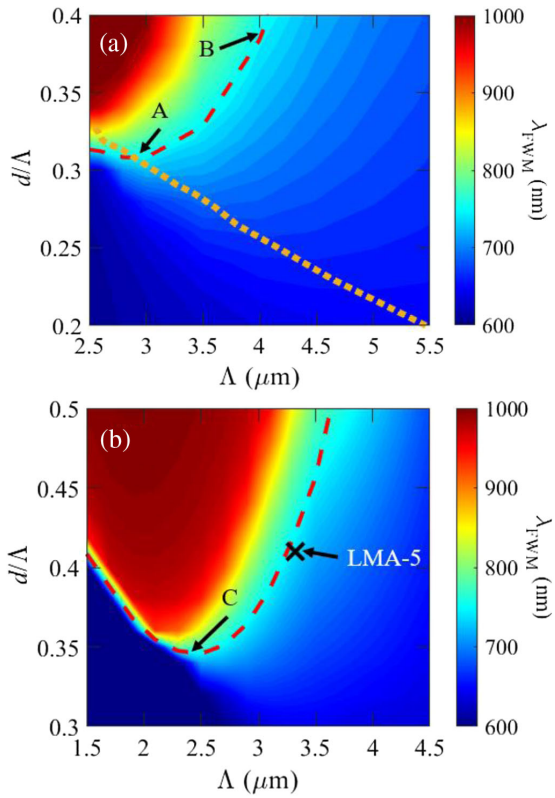

Fig. 1. Four-wave mixing signal wavelength λ_{FWM} using a pump wavelength of (a) 1064 nm and (b) 1030 nm as a function of the pitch Λ and the hole diameter to pitch ratio d/Λ. The red dashed curve shows the contour where $\lambda_{\mathrm{FWM}} = 750$ nm. Points "A" and "C" show the condition where $d\lambda_{\mathrm{FWM}}/d\Lambda = 0$, compared with point "B" where $d\lambda_{\mathrm{FWM}}/d\Lambda$ is not zero. The yellow dotted curve shows the curve along which $d\lambda_{\mathrm{FWM}}/d\Lambda = 0$ for different λ_{FWM}. The black cross shows the parameter location for a measured NKT LMA-5 fiber [30].

However, this derivative remains relatively small compared to other points in the figure. Hence, we expect and will show in Section 4 that the wavelength conversion process in this case will be less sensitive to the variation of pitch along the fiber. We further calculate the curvature of the red dashed curve at points "A" and "C" based on the unit of μm in the x-axis and unitless in the y-axis. We find that the radius of curvature is 8.9 and 5.9 for points "A" and "C," respectively. The configuration represented by point "A" is expected to be more efficient compared with point "C" in terms of conversion efficiency since $d\lambda_{\mathrm{FWM}}/d\Lambda$ is zero with a larger radius of curvature. Hence, we will focus on point "A" for the remaining of the paper. In addition, we also plot the point labeled "B" with a sizable non-zero derivative of $d\lambda_{\mathrm{FWM}}/d\Lambda$. We will compare the conversion efficiency at these two operating points of "A" and "B" in Section 4.

In Fig. 1(a), we also show the yellow dotted curve for the optimal choice of Λ and d/Λ at which $d\lambda_{\mathrm{FWM}}/d\Lambda = 0$ as we vary λ_{FWM}. We further extracted the parameters from the yellow dotted curve and plot Λ and d/Λ as a function of λ_{FWM} in Fig. 2. As the FWM wavelength λ_{FWM} decreases, the fiber pitch Λ should increase, and d/Λ should decrease. This choice minimizes the sensitivity of the FWM process to variations in pitch along the fiber.

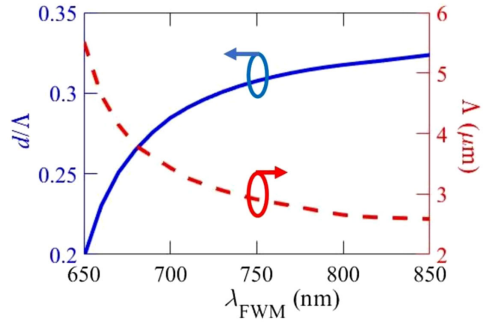

Fig. 2. PCF geometry of average pitch, Λ, and hole diameter to pitch ratio, d/Λ, which is expected to generate a FWM signal insensitive to the random variation of PCF pitch in the longitudinal direction. This figure shows a wide range of λ_{FWM} with the proper choice of PCF geometry.

3. NUMERICAL MODEL

In this section, we will describe our wave propagation model. We use the generalized nonlinear Schrödinger equation (GNLS) to model nonlinear pulse propagation in the optical fiber [24,31,32],

$$\frac{\partial A(z,t)}{\partial z} + \frac{a}{2}A - i\mathrm{IFT}\left\{[\beta(\omega_0+\Omega)-\beta(\omega_0)-\Omega\beta_1(\omega_0)]\tilde{A}(z,\Omega)\right\} = i\gamma\left(1+\frac{i}{\omega_0}\frac{\partial}{\partial t}\right)\left[A(z,t)\int_{-\infty}^{t}R(t-t')|A(z,t')|^2dt'\right], \quad (1)$$

where $A(z, t)$ is the electric field envelope as a function of distance along the fiber z and retarded time t, a is the fiber leakage loss, $\beta(\omega)$ is the wavenumber as a function of frequency, and $\beta_1(\omega) = d\beta/d\omega$ is the inverse group velocity. We use IFT to denote the inverse Fourier transform, where Ω is the transform variable and the tilda indicates the Fourier transform. The third term on the left-hand side of Eq. (1) accounts for linear dispersion, and the right-hand side accounts for the nonlinear contribution. This equation includes several nonlinear optical effects, including self-phase modulation, modulational instability, stimulated Raman scattering, and FWM. Although the FWM process can be simulated using a more simplified equation, we still use the GNLS in order to accurately determine the conversion efficiency, while including other nonlinear effects. The chromatic dispersion for the silica glass material is also included in our simulation [33].

Both continuous wave (CW) and pulsed laser sources have been used to generate shorter wavelengths using FWM [5,34,35]. Generally, picosecond pulse sources with kilowatts of peak power have been used to obtain the highest FWM using short lengths of PCF fiber [35]. Longer nanosecond pulsed or quasi-CW laser sources with lower peak power have several advantages for FWM generation. First, nanosecond to quasi-CW lasers are more commonly available and usually have higher average power than picosecond pulsed sources. Second, it is more expensive to obtain a picosecond pulsed laser that can reach multi-watt average output powers, than for nanosecond and quasi-CW lasers. Third, the peak powers of typical nanosecond and quasi-CW lasers are not as high as the peak powers of picosecond pulsed lasers, so the competing process of SPM plays a limited role. Finally, the low peak power pulsed or quasi-CW lasers also lower the risk of laser damage at the fiber end. On the other hand, longer interaction lengths are often needed when using these lasers. In this case, phase noise and intensity fluctuations relative to the temporal interaction in the fiber becomes important. This nondeterministic behavior makes modeling these sources more challenging. There are several different approximations that have been used to model long pulse and quasi-CW laser sources. One approach is to model these sources as a single frequency laser with random spectral noise [36]. Another approach is to model these sources with a constant temporal power and Gaussian-distributed phase noise, which leads to a Lorentzian-shaped laser spectrum [37,38]. Both these approximations lead to difficulties [31]. Here, we use the approach suggested by Travers *et al*. [31] in which we model a realistic laser. We start with a low power spectrum with completely random noise. We then amplify the spectrum through an active fiber with spectrally dependent gain and gain saturation. We model the Bragg gratings at the end of each amplification pass by using a suitable spectral filter [39,40]. We iterate the spectrum inside the cavity until the output peak power is at the desired level. Using our model, we performed a comparison and obtained good agreement between our simulation results and the results of Travers *et al*. [31]. A bandwidth of 100 pm from the quasi-CW laser is used in this simulation, in agreement with experiments [41,42].

4. RESULTS AND ANALYSIS

A. FWM Spectrum

We carried out wave propagation simulations using Eq. (1) with random variations of Λ, while holding d/Λ constant, as the ratio of pitch to hole diameter is nearly constant when there are variations in Λ [13,20,21]. Figure 3 shows a schematic illustration of the setup used in simulation, which consists of a continuous wave (CW) laser that serves as the pump source, coupled to a photonic crystal fiber (PCF). We used a fiber length of 2 m in our simulation, and we simulated two fibers. Type A fibers have an average pitch of $\Lambda = 2.9$ μm with a fixed $d/\Lambda = 0.31$, while Type B fibers have an average pitch of $\Lambda = 4.0$ μm with a fixed $d/\Lambda = 0.38$. We show both cases in Fig. 1. We used a z-discretization $\Delta z = 20$ μm in our model. The fiber in our simulation was made up of piecewise constant sections of fiber, in which a new pitch was randomly selected every $\Delta L = 15$ cm. For simplicity, we used a uniform distribution with a maximum variation of $\delta = 1\%$ to model the random selection of pitch values along the fiber. We then updated Eq. (1) using the corresponding dispersion, effective area, and nonlinearity. We selected $\Delta L = 15$ cm based on previous results [12]. We have verified that reducing ΔL to 2 cm yields the same behavior that is observed in Fig. 2.

Figure 4 shows the evolution of the spectrum along the fiber for both type A and type B fibers. The growth of short and long wavelength components due to the FWM process occurs along the total fiber length of 2 m, with some depletion of the pump at 1.064 μm. The output wavelengths do not change significantly when the pump peak power varies [7,43,44]. The Raman effect plays a role in the evolution of the spectrum by shifting portions of the spectrum of the anti-Stokes wave to longer wavelengths, which also facilitates the additional generation of the Stokes wave at shorter wavelengths.

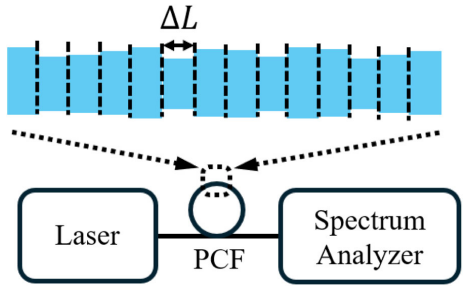

Fig. 3. Schematic illustration of the setup used in the simulation.

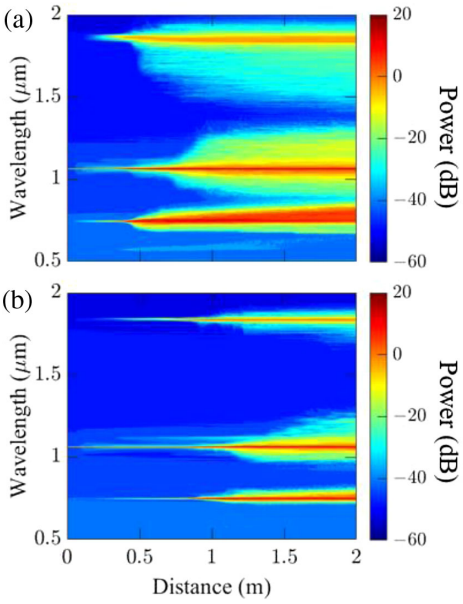

Fig. 4. Power evolution in (a) a type A and (b) a type B fiber. A maximum random variation $\delta = 1\%$ is used in the simulation.

Figure 5 shows the output spectra for both type A and type B fibers whose maximum random variations are $\delta = 0\%$, 1%, and 5%. We ran simulations with 300 fiber realizations, and we show the statistical average for the spectrum in Fig. 5. We use a resolution bandwidth of 1 nm to plot the spectrum. The output spectrum of type A fibers does not change much as δ increases. However, the output spectrum of type B fibers changes noticeably as δ increases from 0 to 5%. These results are consistent with our discussion in Section 2. When we study the FWM process, it is possible to find the PCF geometry with an average pitch and a fixed d/Λ so that FWM is insensitive to the variation of pitch along the fiber longitudinal direction.

B. Sensitivity

We now study the efficiency of FWM as the maximum random variation δ changes. Figure 6 shows the efficiency of the FWM process, which is defined as the ratio of the total output power at wavelengths below 900 nm to the total input power. We again ran simulations with 300 fiber realizations, and we show the statistical average for each data point in Fig. 6. Type B fibers have a lower efficiency than type A fibers even at $\delta = 0$ due to their larger pitch and hole diameter, which implies a larger effective area and a smaller nonlinearity. However, a more important

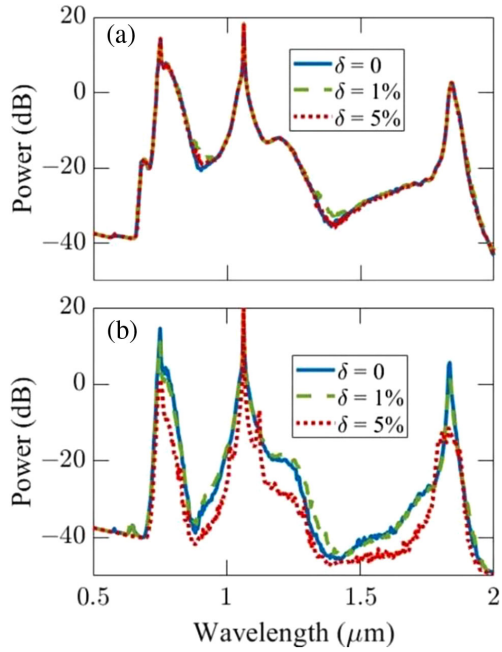

Fig. 5. Output spectra using (a) a type A and (b) a type B fiber with δ equal to 0%, 1%, and 5%.

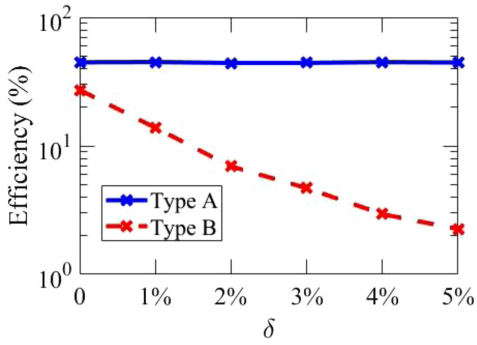

Fig. 6. Efficiency using (a) type A and (b) type B fibers with δ varying from 0 to 5%. We used 300 fiber realizations to estimate each of the data points for the efficiency.

observation is the severe degradation in the efficiency of type B fibers when δ increases, while there is almost no degradation in the efficiency of type A fibers. For type A fibers, the efficiency only changes from 45% to 44% when δ increases from 0 to 5%. Hence, the FWM process is insensitive to the fiber variation for the type A fibers. On the other hand, for type B fibers, the efficiency drops by an order of magnitude when δ increases from 0 to 5%.

Figure 7 illustrates the efficiency as a function of pitch Λ. The corresponding d/Λ is selected based on the red dashed curve in Fig. 1(a). We ran 10 different fiber realizations for each pitch Λ value. The efficiency is plotted as crosses in Fig. 7. Some of the crosses overlap when the efficiency is small. The spread of individual data points implies a spread of the FWM efficiency due to the fiber variation along the longitudinal direction. According to Fig. 1, if we vary pitch Λ by 5%, the phase matching condition will lead to generation of slightly different FWM wavelengths. In addition, the generalized nonlinear Schrödinger

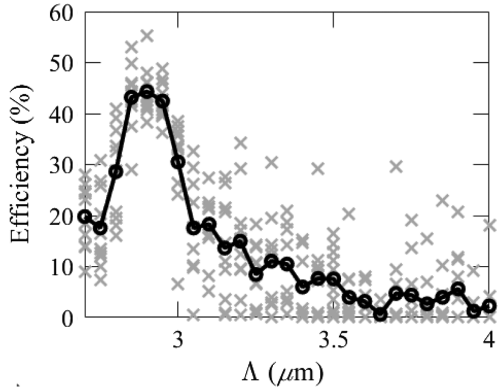

Fig. 7. Efficiency as a function of pitch Λ. The corresponding d/Λ is selected based on the red dashed curve in Fig. 1(a). The cross markers indicate 10 fiber realizations for each pitch Λ. The circle markers show the average efficiency of 10 fiber realizations, $\delta = 5\%$.

equation (GNLS) describes a complicated process that includes the physical effects of self-phase modulation, cross-phase modulation, modulation instabilities, stimulated Raman scattering, and FWM. The small change in the generated FWM wavelengths leads to a spread of the efficiency, as shown in Fig. 7. The circles indicate the average efficiency for each pitch Λ value. The figure shows that a pitch of 2.9 μm is optimal. This optimal point is identified as point "A" on a red dashed curve referenced in Fig. 1(a). The optimized structure of optical fibers can lead to enhanced performance for specific nonlinear applications.

5. CONCLUSION

In this paper, we investigated the dependence of the FWM conversion efficiency on the geometric parameters (pitch and hole diameter) of a PCF in which the pitch is randomly varying along the fiber while the ratio of the hole diameter to the pitch remains constant. We found that the conversion efficiency is maximized by choosing the parameters so that the derivative of the FWM wavelength λ_{FWM} with respect to the pitch is zero. The maximum average conversion efficiency reaches 45% with a fiber pitch Λ of 2.9 μm and a hole diameter to pitch ratio d/Λ of 0.31. With this choice, the sensitivity of λ_{FWM} to changes in the pitch is reduced. We applied this criterion to a pump at 1064 nm and a range of visible signal wavelengths from 650 to 850 nm. At an output signal wavelength of 750 nm, we contrasted in detail the behavior of a fiber (labeled type A) that obeys this criterion to a fiber (labeled type B) that does not. We found that while the conversion efficiency of the type B fibers dramatically decreases as the random variation increases, the conversion efficiency of type A fibers remains almost flat.

While our focus in this paper was on a relatively simple PCF that consisted of five air hole rings and a single pump wavelength, corresponding to the output of a Yb-doped fiber amplifier, we expect that our results will have a significantly greater range of applications. It is difficult to reduce the variation of the geometric parameters of a PCF below some lower limit. Hence, it is appealing to design the mean parameters of the fiber so that the FWM mixing process is insensitive to these variations.

Funding. U.S. Naval Research Laboratory (N00173-19-S-BA01).

Acknowledgment. Work at UMBC is supported by the U.S. Naval Research Laboratory, grant no. N00173-19-S-BA01.

Disclosures. The authors declare no conflicts of interest.

Data availability. Data underlying the results presented in this paper are not publicly available at this time but may be obtained from the authors upon reasonable request.

REFERENCES

1. M. N. Zervas and C. A. Codemard, "High power fiber lasers: a review," IEEE J. Sel. Top. Quantum Electron. **20**, 0904123 (2014).
2. C. Jauregui, J. Limpert, and A. Tunnermann, "High-power fibre lasers," Nat. Photonics **7**, 861–867 (2013).
3. D. J. Richardson, J. Nilsson, and W. A. Clarkson, "High power fiber lasers: current status and future perspectives," J. Opt. Soc. Am. B **27**, B63–B92 (2010).
4. G. P. Agrawal, *Nonlinear Fiber Optics* (Academic, 2019).
5. J. E. Sharping, M. Fiorentino, A. Coker, *et al.*, "Four-wave mixing in microstructure fiber," Opt. Lett. **26**, 1048–1050 (2001).
6. W. J. Wadsworth, N. Joly, J. C. Knight, *et al.*, "Supercontinuum and four-wave mixing with Q-switched pulses in endlessly single-mode photonic crystal fibres," Opt. Express **12**, 299–309 (2004).
7. L. Lavoute, J. C. Knight, P. Dupriez, *et al.*, "High power red and near-IR generation using four wave mixing in all integrated fibre laser systems," Opt. Express **18**, 16193–16205 (2010).
8. M. E. Marhic, K. K. Y. Wong, and L. G. Kazovsky, "Wide-band tuning of the gain spectra of one-pump fiber optical parametric amplifiers," IEEE J. Sel. Top. Quantum Electron. **10**, 1133–1141 (2004).
9. A. Y. H. Chen, G. K. L. Wong, S. G. Murdoch, *et al.*, "Widely tunable optical parametric generation in a photonic crystal fiber," Opt. Lett. **30**, 762–764 (2005).
10. J. G. Koefoed, S. M. M. Friis, J. B. Christensen, *et al.*, "Spectrally pure heralded single photons by spontaneous four-wave mixing in a fiber: reducing impact of dispersion fluctuations," Opt. Express **25**, 20835–20849 (2017).
11. J. S. Y. Chen, S. G. Murdoch, R. Leonhardt, *et al.*, "Effect of dispersion fluctuations on widely tunable optical parametric amplification in photonic crystal fibers," Opt. Express **14**, 9491–9501 (2006).
12. R. J. A. Francis-Jones and P. J. Mosley, "Characterisation of longitudinal variation in photonic crystal fibre," Opt. Express **24**, 24836–24845 (2016).
13. B. Stiller, S. M. Foaleng, J. C. Beugnot, *et al.*, "Photonic crystal fiber mapping using Brillouin echoes distributed sensing," Opt. Express **18**, 20136–20142 (2010).
14. E. Ciaramella and M. Tamburrini, "Modulation instability in long amplified links with strong dispersion compensation," IEEE Photonics Technol. Lett. **11**, 1608–1610 (1999).
15. N. J. Smith and N. J. Doran, "Modulational instabilities in fibers with periodic dispersion management," Opt. Lett. **21**, 570–572 (1996).
16. S. G. Murdoch, R. Leonhardt, J. D. Harvey, *et al.*, "Quasi-phase matching in an optical fiber with periodic birefringence," J. Opt. Soc. Am. B **14**, 1816–1822 (1997).
17. F. K. Abdullaev, S. A. Darmanyan, A. Kobyakov, *et al.*, "Modulational instability in optical fibers with variable dispersion," Phys. Lett. A **220**, 213–218 (1996).
18. M. Karlsson, "Four-wave mixing in fibers with randomly varying zero-dispersion wavelength," J. Opt. Soc. Am. B **15**, 2269–2275 (1998).
19. M. Farahmand and M. de Sterke, "Parametric amplification in presence of dispersion fluctuations," Opt. Express **12**, 136–142 (2004).
20. C. R. Petersen, R. D. Engelsholm, C. Markos, *et al.*, "Increased mid-infrared supercontinuum bandwidth and average power by tapering large-mode-area chalcogenide photonic crystal fibers," Opt. Express **25**, 15336–15347 (2017).
21. J. Hu, B. S. Marks, C. R. Menyuk, *et al.*, "Pulse compression using a tapered microstructure optical fiber," Opt. Express **14**, 4026–4036 (2006).
22. Z. Holdynski, M. Napierala, P. Mergo, *et al.*, "Experimental investigation of supercontinuum generation in photonic crystal fibers pumped with sub-ns pulses," J. Lightwave Technol. **33**, 2106–2110 (2015).

23. R. W. Boyd, *Nonlinear Optics* (Academic, an imprint of Elsevier, 2020).
24. J. Hu, C. R. Menyuk, L. B. Shaw, *et al.*, "Maximizing the bandwidth of supercontinuum generation in As_2Se_3 chalcogenide fibers," Opt. Express **18**, 6722–6739 (2010).
25. K. Saitoh and M. Koshiba, "Leakage loss and group velocity dispersion in air-core photonic bandgap fibers," Opt. Express **11**, 3100–3109 (2003).
26. A. Alismail, H. C. Wang, G. Barbiero, *et al.*, "Multi-octave, CEP-stable source for high-energy field synthesis," Sci. Adv. **6**, 3408 (2020).
27. A. Rovere, Y. G. Jeong, R. Piccoli, *et al.*, "Generation of high-field terahertz pulses in an HMQ-TMS organic crystal pumped by an ytterbium laser at 1030 nm," Opt. Express **26**, 2509–2516 (2018).
28. Y. Orii, K. Yoshii, K. Kohno, *et al.*, "High-power deep-ultraviolet light generation at 266 nm from frequency quadrupling of a picosecond pulsed 1064 nm laser with a Nd:YVO_4 amplifier pumped by a 914 nm laser diode," Opt. Express **31**, 14705–14714 (2023).
29. Y. Ren, X. Zhao, E. W. Hagley, *et al.*, "Ambient-condition growth of high-pressure phase centrosymmetric crystalline KDP microstructures for optical second harmonic generation," Sci. Adv. **2**, 1600404 (2016).
30. Y. Tao and S. P. Chen, "All-fiber high-power linearly polarized supercontinuum generation from polarization-maintaining photonic crystal fibers," High Power Laser Sci. Eng. **7**, e28 (2019).
31. J. C. Travers, A. B. Rulkov, B. A. Cumberland, *et al.*, "Visible supercontinuum generation in photonic crystal fibers with a 400W continuous wave fiber laser," Opt. Express **16**, 14435–14447 (2008).
32. R. J. Weiblen, A. Docherty, J. Hu, *et al.*, "Calculation of the expected bandwidth for a mid-infrared supercontinuum source based on As_2S_3 chalcogenide photonic crystal fibers," Opt. Express **18**, 26666–26674 (2010).
33. I. H. Malitson, "Interspecimen comparison of refractive index of fused silica," J. Opt. Soc. Am. **55**, 1205–1209 (1965).
34. K. Inoue, "4-wave-mixing in an optical fiber in the zero-dispersion wavelength region," J. Lightwave Technol. **10**, 1553–1561 (1992).
35. J. C. Delagnes, R. Royon, J. Lhermite, *et al.*, "High-power widely tunable ps source in the visible light based on four wave mixing in optimized photonic crystal fibers," Opt. Express **26**, 11265–11275 (2018).
36. S. M. Kobtsev and S. V. Smirnov, "Modelling of high-power supercontinuum generation in highly nonlinear, dispersion shifted fibers at CW pump," Opt. Express **13**, 6912–6918 (2005).
37. A. Mussot, E. Lantz, H. Maillotte, *et al.*, "Spectral broadening of a partially coherent CW laser beam in single-mode optical fibers," Opt. Express **12**, 2838–2843 (2004).
38. M. H. Frosz, O. Bang, and A. Bjarklev, "Soliton collision and Raman gain regimes in continuous-wave pumped supercontinuum generation," Opt. Express **14**, 9391–9407 (2006).
39. T. Erdogan, "Fiber grating spectra," J. Lightwave Technol. **15**, 1277–1294 (1997).
40. M. Toba, F. M. Mustafa, and T. M. Barakat, "New simulation and analysis fiber Bragg grating: narrow bandwidth without side lobes," J. Phys. Commun. **4**, 075018 (2020).
41. R. Royon, J. Lhermite, L. Sarger, *et al.*, "High power, continuous-wave ytterbium-doped fiber laser tunable from 976 to 1120 nm," Opt. Express **21**, 13818–13823 (2013).
42. E. A. Zlobina, S. I. Kablukov, and S. A. Babin, "Phase matching for parametric generation in polarization maintaining photonic crystal fiber pumped by tunable Yb-doped fiber laser," J. Opt. Soc. Am. B **29**, 1959–1967 (2012).
43. C. Jauregui, A. Steinmetz, J. Limpert, *et al.*, "High-power efficient generation of visible and mid-infrared radiation exploiting four-wave-mixing in optical fibers," Opt. Express **20**, 24957–24965 (2012).
44. D. Nodop, C. Jauregui, D. Schimpf, *et al.*, "Efficient high-power generation of visible and mid-infrared light by degenerate four-wave-mixing in a large-mode-area photonic-crystal fiber," Opt. Lett. **34**, 3499–3501 (2009).